Effect of scandia content on the hot corrosion behavior of Sc2O3 and Y2O3 co-doped ZrO2 in Na2SO4 + V2O5 molten salts at 1000 °C

Chao Chen, Tianquan Liang, Yan Guo, Xiyong Chen, Quanyan Man, Xiuhai Zhang, Jianmin Zeng, Vincent Ji

Effect of Scandia content on the hot corrosion behavior of Sc_2O_3 and Y_2O_3 co-doped ZrO_2 in Na_2SO_4 + V_2O_5 molten salts at 1000 °C

Chao Chen[a], Tianquan Liang[a,b,c,d *], Yan Guo[a], Xiyong Chen [a,b,*], Quanyan Man[a], Xiuhai Zhang[a,b,c], Jianmin Zeng[a,b,c], Vincent Ji[d]

[a] School of Resources, Environment and Materials, Guangxi University, Nanning 530004, PR China

[b] Guangxi Key Laboratory of Processing for Non-ferrous Metals and Featured Materials, Nanning 530004, Guangxi, PR China

[c] Center of Ecological Collaborative Innovation for Aluminum Industry in Guangxi, Nanning 530004, PR China

[d] ICMMO/SP2M, UMR CNRS 8182, Université Paris-Sud, 91405 Orsay Cédex, France

*To whom all correspondence should be addressed.

E-mail: liangtianquan@gxu.edu.cn, xiyongchen@gxu.edu.cn

ABSTRACT

The effect of Sc_2O_3 content on the hot corrosion behavior of *x* mol.% Sc_2O_3-1.5 mol.% Y_2O_3 co-doped ZrO_2 ceramics (ScYSZ) in Na_2SO_4 + V_2O_5 (50/50 wt.%) molten salts at 1000 °C was investigated. The experiments revealed that the hot corrosion resistance and phase stability of the ScYSZ ceramics increase with the Sc_2O_3 content as results of the enhanced strength of rare earth-oxygen bond and the increased prohibition effect on the vanadate penetration due to the small ionic radius of Sc^{3+} and the weak reactivity of Sc_2O_3 with vanadates. The hot corrosion mechanism was also discussed.

Keywords: Scandia doped yittria stabilized zirconia; Phase stability; Hot corrosion; Sulfate and vanadate molten salts; Mechanism

1. Introduction

Thermal barrier coatings (TBCs) are widely used to protect hot sectional components of gas turbines from high temperature attack, and therefore to increase the operation temperature and thermal efficiency [1, 2]. The commercial 6-8 wt.% Y_2O_3 partially stabilized ZrO_2 (YSZ) is currently the primary choice for the TBCs topcoat due to its low thermal conductivity, comparative thermal expansion coefficient with the substrate, and excellent thermal shock resistance [3, 4]. However, further applications of YSZ are limited by the destructive tetragonal-to-monoclinic phase transformation and the serious sintering problem when the working temperature exceeds 1200 °C [5-7]. In addition, low quality fuels used in gas turbines or diesel engines usually contain impurities such as vanadium, sulfur and sodium. These impurities form Na_2SO_4 and $NaVO_3$, which will condense on the surface of TBCs and then form low-melting-point molten salts at the temperature of 600-1050 °C [8-10].

The molten salt will penetrate into the TBCs through the splat boundaries and open pores of YSZ coatings prepared by the air plasma spraying (APS), or through the inter-columnar gaps of ceramic coatings by the electron beam physical vapor deposition (EB-PVD) or plasma spray physical vapor deposition (PS-PVD). The penetrated corrosive salts would react with the stabilizers in ZrO_2, and further result in the leaching of stabilizers. As a result, non-transformable tetragonal zirconia (t'-ZrO_2) and the transformable tetragonal zirconia (t-ZrO_2) phases would transform to monoclinic zirconia (m-ZrO_2) phase accompanying with 4 % volume expansion,

which leads to the formation of macro-cracks and degradation of TBCs [11-13].

In recent years, a great deal of researches have been conducted to improve hot corrosion resistance of YSZ against sulfate and vanadate molten salts by doping rare earth oxides or other oxides such as CeO_2, TiO_2, Gd_2O_3, Yb_2O_3, Al_2O_3, HfO_2, Sc_2O_3, Ta_2O_5, etc [9,13-18]. Studies showed that the Sc_2O_3 and Y_2O_3 co-doped ZrO_2 (ScYSZ) was a promising material for TBCs application owing to its low thermal conductivity, long thermal cycling lifetime and excellent phase stability at ultra-high temperature above 1400 °C [19-24], as well as its outstanding hot corrosion resistance to V_2O_5 or Na_2SO_4 + V_2O_5 molten salts [24-27]. The significantly better tetragonal phase stability of Sc_2O_3 and Y_2O_3 co-doped ZrO_2 over YSZ at 1400 °C has been verified when the total stabilizer content is around 7 mol.% with relatively less Y_2O_3 (0.17 to 1.36 mol.%) [21]. Leoni [23] also claimed that the 6.57 mol.% Sc_2O_3-1.00 mol.% Y_2O_3 doped ZrO_2 APS coating has excellent tetragonal phase stability after exposure to 1400 °C for 1500 h. Liu et al. [15] reported that 8 mol.% Sc_2O_3-0.6 mol.% Y_2O_3-ZrO_2 TBCs exhibited superior phase stability after 300 h annealing at 1500 °C. Literature [23] showed that the 7.0 Sc_2O_3-0.5 Y_2O_3-ZrO_2, 6.5 Sc_2O_3-1.0 Y_2O_3-ZrO_2 and 5.5 Sc_2O_3-2.0 Y_2O_3-ZrO_2 (in mol.%) ceramics had good phase stability after 200 h annealing at 1500 °C with the exception of 5.5 Sc-2.0 Y-ZrO_2 in which about 4.6 mol.% monoclinic phase appears in the sample. All of these studies indicate that the Sc_2O_3 and Y_2O_3 co-doped ZrO_2 (ScYSZ) has excellent tetragonal phase stability at ultra-high temperature when total stabilizer concentration reaches 7.0 mol.% and the content of Y_2O_3 is within the range of 0.5-2.0 mol.%. The high tetragonal phase stability of ScYSZ at high stabilizer concentrations can be strongly associated with the low crystal tetragonality (*c*/*a* ratio, *c* and *a* are the lattice

parameters). Jones [21] and Leoni [23] suggested that the crystal tetragonality decreases with the increase of the total stabilizer content within a certain concentration range, and lower tetragonality generally indicates the better tetragonal phase stability at high temperature.

Doping of Sc_2O_3 in YSZ can also improve the hot corrosion resistance significantly over YSZ. Jones[24] reported that Sc_2O_3-stabilized ZrO_2 (ScSZ) gave no detectable reaction or destabilization in $NaVO_3$ molten salt for 160 h at 900 °C since Sc_2O_3 has the strongest acidity of the rare earth and its effective stability to t-ZrO_2. And thus the Sc_2O_3 and Y_2O_3-stabilized ZrO_2 (SYSZ) is substantially more resistant to vanadate hot corrosion than Y_2O_3-stabilized ZrO_2 in corrosive molten salts at high temperatures of 700 °C-900 °C. The air plasma spraying (APS) prepared 3.4 mol.% Sc_2O_3-0.6 mol.% Y_2O_3-ZrO_2 coating also exhibited better hot corrosion resistance than YSZ coating in Na_2SO_4 + V_2O_5 molten salts at 910 °C [26]. Liu et al. [27] reported that 8 mol.% Sc_2O_3-0.6 mol.% Y_2O_3-ZrO_2 TBCs showed superior hot corrosion resistance compared with YSZ coating in the presence of Na_2SO_4 + V_2O_5 molten salts at 1000 °C. These results show that Sc_2O_3 and Y_2O_3 co-stabilized ZrO_2 has outstanding hot corrosion resistance to Na_2SO_4 + V_2O_5 molten salts at high temperatures.

In all, many research efforts pointed out that the excellent tetragonal phase stability of ScYSZ at ultra-high temperature (e. g. 1500 °C) can be achieved when the total stabilizer concentration reaches around 7-7.5 mol.% which the Y_2O_3 content as high as 2.0 mol.%. As for the hot corrosion resistance, most of the works focused on the corrosion properties of the ScYSZ ceramics containing relatively high level of Sc_2O_3 and low Y_2O_3 content. Very few studies have been carried out on the hot corrosion

resistance of the ScYSZ ceramics with relatively high content of Y_2O_3 stabilizer (e. g. 1.5 or 2.0 mol.%), possibly because of the fact that Y_2O_3 is easy to react with the molten salts of Na_2SO_4 + V_2O_5 at high temperatures and then accelerates the degradation of doped ZrO_2 ceramics in corrosive environments. To further understand the hot corrosion resistance of the Sc_2O_3 and Y_2O_3 doped ZrO_2 with high amount of Y_2O_3 (e. g. 1.5 mol.%) and the effect of the Sc_2O_3 content on the hot corrosion resistance of *x* mol.% Sc_2O_3 and 1.5 mol.% Y_2O_3 co-doped ZrO_2 (*x*Sc1.5YSZ) against Na_2SO_4 + V_2O_5 molten salts at 1000 °C, the phase stability and the corrosion behavior of the *x*Sc1.5YSZ ceramics are investigated in this work. The corrosive mechanism of xSc1.5YSZ in the Na_2SO_4 + V_2O_5 molten salts is also discussed.

2. Experimental procedures

2.1. Sample preparation

xSc_2O_3-1.5Y_2O_3-ZrO_2 (x=4.5, 5.5, 6.5, in mol.%) and 4.5 mol.% Y_2O_3-ZrO_2 powders were prepared by a chemical co-precipitation and calcination method. $ZrOCl_2 \cdot 8H_2O$, $YCl_3 \cdot 6H_2O$ and $ScCl_3 \cdot 6H_2O$ were selected as raw materials, and were dissolved in deionized water respectively. Then the solutions were mixed and stirred to yield a 0.2mol/L homogeneous solution together with 2 wt.% PEG-2000 as the dispersing agent. The mixed homogeneous solution was gently agitated in a 60 °C water bath and added with an appropriate amount of ammonia solution drop-wisely at a speed of 5 mL/min to get precipitate. The final PH value of the mixture solution was controlled at the range of 10-11 by adding additional ammonia. After complete reaction, the precipitate was filtered and washed thoroughly by deionized water and alcohol for several times until the turbidity didn't appear in the washed water when adding 1.0 mol/L $AgNO_3$ solution. The obtained precipitate was dried at 110 °C for 20 h, and

then ground into powders. The powders were calcined for 5 h at 900 °C for crystallization. The samples for the hot corrosion tests were obtained by mechanically pressing the powders into discs with 15 mm in diameter and 2 mm in thickness under 300 MPa for 10 min. The disc samples were later sintered in air for 5 h at 1500 °C.

2.2. Hot corrosion tests

The hot corrosion tests of the samples were conducted at 1000 °C in an ambient atmosphere. The samples were subjected to a 4-session hot corrosion process with 25 hours for each session. Prior to each session of hot corrosion test, the samples were rinsed thoroughly with deionized water and dried thereafter. The sample surfaces were then uniformly coated with a concentration of 10 $mg \cdot cm^{-2}$ of corrosive salts containing 50 wt.% Na_2SO_4 + 50 wt.% V_2O_5.

2.3. Characterization

The phase constitutions of the as-prepared samples and the corroded surfaces of YSZ and ScYSZ samples were characterized by X-ray diffraction (XRD, Model D/MAX 2500, Rigaku Co. Ltd., Japan) with Cu Kα radiation λ=1.5406 Å at a scan speed of 2 deg./min with a step size of 0.0065 deg. The volume fractions of the monoclinic (m), cubic (c), and tetragonal (t) phases are calculated by using the following equations [28, 29]:

$$\frac{M_m}{M_{c,t}} = 0.82\,\frac{I_m(\bar{1}11) + I_m(111)}{I_{c,t}(111)} \tag{1}$$

$$\frac{M_c}{M_t} = 0.88\,\frac{I_c(400)}{I_{t1}(004) + I_{t1}(400) + I_{t2}(004) + I_{t2}(400)} \tag{2}$$

$$\frac{M_{t1}}{M_{t2}} = \frac{I_{t1}(004) + I_{t1}(400)}{I_{t2}(004) + I_{t2}(400)} \tag{3}$$

$$M_t = M_{t1} + M_{t2} \quad (4)$$

$$M_m + M_c + M_{t1} + M_{t2} = 1 \quad (5)$$

where M_m, M_c and M_t are the volume fractions of m, c, t phases, respectively. $M_{c,t}$ is the total amount of the volume fractions of the c, t phases, and I refers to the integral intensity corresponding to the peaks concerned. The subscribes, t_1 and t_2, represent the possible coexisting different t phases in the samples, i.e., the t and t' phases as described in [23] or the stabilizer-rich and -poor phases as in [23, 29].

To further analyze the phase transformation and the phase constitution in the ScYSZ ceramics, Raman spectrum measurements were conducted with a microscopic confocal Raman spectrometer (inVia Reflex, Renishaw, UK) using 532 nm excitation from an argon ion laser. The surface and cross-sectional morphologies of the specimens were obtained by a field emission scanning electron microscope (FESEM, Hitachi SU8020, Japan) equipped with an energy dispersive spectroscopy (EDS, Oxford X-MAX 80). The samples were sputtered with Au before the SEM observation.

3. Results and discussion

3.1 Phase constitution analysis

The XRD patterns of the as-prepared ceramics are shown in Fig. 1. One can clearly see that all the YSZ and ScYSZ samples are mainly composed of tetragonal zirconia phase (t-ZrO_2) according to Fig. 1a. No Sc_2O_3 and Y_2O_3 phases are detected. It indicates that all the rare earth stabilizers were completely dissolved in ZrO_2 crystals. It should be noted that the diffraction peaks shift to the right as the Sc_2O_3 content increases in the ZrO_2 ceramics (Fig. 1a). The rightward peak shifting with Sc_2O_3

content in the ceramic composition mainly results from the shrinkage of the unit cell due to the reduced average rare earth anion radius [29, 30]. The lattice parameters of the as-prepared ScYSZ ceramics evaluated by the Rietveld refinement method are shown in Table 1. The data indicates that the YSZ and 4.5Sc1.5YSZ ceramics in this work have two tetragonal phases as shown in Fig. 1b-d, denoted as t_1 and t_2 phases. Note that t_1 and t_2 phases have the same tetragonal structure but different lattice parameters. The phase with a large tetragonality value ($c/\sqrt{2}a$), i.e., t_2 phase in this work, may refer to the "low-stabilizer" phase or RE-poor t-phase, and the other phase (t_1) with a small value is the "high-stabilizer" phase or RE-rich t-phase, as explained in literatures [23, 29]. The contents of t_1 phases are evaluated around 40 vol.% and 65 vol.% in the YSZ and 4.5Sc1.5YSZ ceramics, respectively. For the 5.5Sc1.5YSZ and 6.5Sc1.5YSZ ceramics, single t_1 phase structure can fit the corresponding XRD patterns very well. The results give a clue that increasing the stabilizer content in zirconia can result in an increased amount of t_1 phase in the sample. Pure t_1 phase can be produced even when the total stabilizer amount in zirconia is more than 7 mol.%.

Fig. 2 shows the XRD patterns obtained from the surface of specimens after hot corrosion in $Na_2SO_4 + V_2O_5$ molten salts at 1000 °C for different hours. And Fig. 3 shows the calculated amounts of the m-ZrO_2 phases in the specimens after corrosion according to Eq. (1). For YSZ, serious corrosion occurred when the ceramic exposed to the molten salts for only 25 h at 1000 °C. The corrosion products are mainly identified as YVO_4 and m-ZrO_2 phases (Fig. 2a). The amount of the corrosion product YVO_4 in YSZ increases with the corrosion time as evidenced by the increased diffraction peak intensity at about 25°. The content of the m-ZrO_2 phase is about 94 vol.% (Table 2 and Fig. 3). It indicates that Y^{3+} ions are easy to leach from the surface

layer of the t-ZrO_2 phase. The leached Y^{3+} later reacts with the corrosive salts to form YVO_4. This results in the easy degradation of 4.5YSZ. 50 h corrosion can completely destroy the surface of the YSZ sample as the amount of the m-ZrO_2 phase becomes 100 vol.%.

The attack of the molten salts to the 4.5Sc1.5YSZ and 5.5Sc1.5YSZ samples at elevated temperature is also serious. According to Figs. 2b and c, significant amounts of m-ZrO_2 phases can be detected after 100h corrosion, which are 84 vol.% and 77 vol.%, respectively. Nevertheless, the overall corrosion processes for the 4.5Sc1.5YSZ and 5.5Sc1.5YSZ samples are less aggressive when compared to YSZ. Large quantities of tetragonal phases still remain in 4.5Sc1.5YSZ and 5.5Sc1.5YSZ after 50 h corrosion, and the amounts of the m-ZrO_2 phases in these samples are roughly 45 vol.% (Table 2 and Fig. 3). Both the samples appear a very close anti-corrosion behavior with slightly more severe corrosion effect on 4.5Sc1.5YSZ than 5.5Sc1.5YSZ during the first 75 h corrosion process in which the amount difference of the m-ZrO_2 phases in these two samples remains around 3 vol.%. In other words, the amount increase of the m-ZrO_2 phase with corrosion time in these two samples is similar. However, the most serious corrosion may occur during the second 25 h hot corrosion session in which the amount of m-ZrO_2 phase increases ~29 vol.% and the corresponding amount increase reduces in the later corrosion sessions. Additionally, YVO_4 is also found as one of the main corrosion products on the surfaces of the corroded 4.5Sc1.5YSZ and 5.5Sc1.5YSZ ceramics. These results show that the tetragonal phases in the 4.5Sc1.5YSZ and 5.5Sc1.5YSZ ceramics can also be degraded dramatically after 100h hot corrosion under the corrosive condition designed in this work.

Alternatively, the 6.5Sc1.5YSZ sample shows excellent corrosion resistance to the $Na_2SO_4 + V_2O_5$ molten salts at 1000 °C (Fig. 2d and Fig. 3, Table 2). There is no any detectable m-ZrO_2 phase in the XRD profiles of the samples obtained from the starting 50 h corrosions. Only trace amounts (less than 1 vol.%) of m-ZrO_2 phase can be observed in the further corroded samples. Similarly, only small amount of YVO_4 can be detected in the corroded 6.5Sc1.5YSZ samples. The result that the 100 h-corroded 6.5Sc1.5YSZ ceramics still retain the primary RE-rich t-ZrO_2 phase indicates that the ceramics is almost totally immune to the $Na_2SO_4 + V_2O_5$ molten salts at 1000 °C.

Raman spectrum measurements were conducted to further analyze the phase transformation behavior of the ceramics in this work. Fig.4 shows the Raman spectra of YSZ and ScYSZ ceramics after hot corrosion in $Na_2SO_4 + V_2O_5$ molten salts at 1000 °C for 100 h. According to Fig. 4, Raman reflections at ~175 cm^{-1}, ~190 cm^{-1}, ~331 cm^{-1}, ~376 cm^{-1} and ~474 cm^{-1} can be ascribed to m-ZrO_2 [31, 32], while those at ~146 cm^{-1}, ~258 cm^{-1} and ~636 cm^{-1} can be assigned to the t-ZrO_2 phases [32-34]. No cubic zirconia (c-ZrO_2) phase was detected according to Fig. 4. The characteristic Raman reflections for YVO_4 typically locate at ~258 cm^{-1}, ~378 cm^{-1}, ~815 cm^{-1}, ~839 $cm^{-1}$and ~892 cm^{-1} [35]. It can be seen that the amounts of the m-ZrO_2 phase and YVO_4 decrease while that of t-ZrO_2 phase increases with the increase of the Sc_2O_3 content. The 6.5Sc1.5YSZ sample shows excellent corrosion resistance to the $Na_2SO_4 + V_2O_5$ molten salts, which is consistent with the previous XRD analysis.

The phase stability of the ZrO_2 ceramic could be clarified by the Y_2O_3- and Sc_2O_3-ZrO_2 phase diagrams [23] (Fig. 5). While a single tetragonal phase can be obtained by

adding more than 3.5 mol. % of Y_2O_3 to ZrO_2 at room temperature, it requires at least 6.5 mol.% for Sc_2O_3 to get a single t-ZrO_2 phase (Fig. 5b). Rather, a single t-ZrO_2 phase can also be produced when the doping amount of Sc_2O_3 reduces to 5.5 mol.% at high temperature, the materials will separate into t-ZrO_2 and m-ZrO_2 phases at room temperature. Fortunately, reports indicated that little amount of Y_2O_3 addition can help increase the stability of t-ZrO_2 phase when decreasing the Sc_2O_3 content in the Sc_2O_3-ZrO_2 ceramics [36, 37]. This is the exact case for the 4.5Sc-ZrO_2 sample investigated in this work, in which the tetragonal phase is obtained at room temperature with only 1.5 mol.% Y_2O_3 addition.

It is also reported that the ionic radius and the content of the substitutional rare earth elements (RE) have essential impacts on the phase stability and anti-corrosion performance of zirconia ceramics at elevated temperatures due to the lattice distortion and change of M-O bonding (M stands for a metal element) [38-41]. The effective radii of cation ions (8-fold coordination) in the ScYSZ ceramics are 0.084 nm, 0.102 nm and 0.087 nm for Zr^{4+}, Y^{3+} and Sc^{3+} [42], respectively. Since the radius of Y^{3+} is larger than that of Zr^{4+}, the average M-O bond length would increase when zirconia is stabilized with Y_2O_3, and therefore the lattice expand. On the opposite, the smaller radius of Sc^{3+} relative to that of Zr^{4+} will lead to the decrease of M-O bond length and therefore the lattice shrinks. Indeed, the variation of the M-O bond length upon the rare earth doping in ZrO_2 has been frequently reported in literature [38, 40]. Reduction in the M-O bond length often results in the decrease of the cell parameters, as seen in Table 1, and the increase of the binding energy [40]. Stronger bonds in Sc_2O_3 co-doped Y_2O_3 stabilized ZrO_2 most likely enhance its ability to prevent the leaching of Y^{3+} from the crystals, and therefore increase the anti-corrosion capability

of *x*Sc1.5YSZ ceramics. Furthermore, the ionic radius of Sc^{3+} is close to that of Zr^{4+}, which can reduce the size misfit between the Sc^{3+} and Zr^{4+} ions. This leads to lowering the driving force for the phase transformation [29], and further helps to increase the phase stability.

3.2. Hot corrosion behavior analysis

Figs. 6a and b present the surface morphologies of YSZ ceramics after 100 h hot corrosion in Na_2SO_4 + V_2O_5 molten salts. Many large bar-shaped corrosion products with various sizes could be clearly observed sitting on the sample surface. A magnified view indicates the surface is mainly consisting of small polyhedral particles with many fine needle-like phases filling in-between the particles. The needle-like phases are considered to be the newly formed corrosion products as the bar-shaped ones. EDS analysis on Region B in Fig. 6b indicates the bar-shaped materials has the chemical composition of YVO_4, as listed in Table 3. Alternatively, the constitutional elements of the substrate surface (e.g. region A in Fig. 6a) are mainly Zr and O with trace amount of Vanadium. No any sign of yttrium can be detected at the surface of the YSZ ceramics after 100h corrosion. Along with the XRD characterization as shown in Fig. 2a, the surface phase can be determined as m-ZrO_2 phase.

Instead of the bar-shaped corrosion products found on the surface of the corroded YSZ ceramics, the corrosion products on the 4.5Sc1.5YSZ sample mainly present granular shapes after 100 h corrosion in the Na_2SO_4 + V_2O_5 molten salts (Figs. 6 c and d). The chemical composition of these granular corrosion products can be assigned to YVO_4 as well according to the EDS elemental characterization (Table 3). Since little Zr (0.7 at.%) and Sc (1.5 at.%) can be detected, the granular particles may contain

very small amounts of ZrO_2 and Sc_2O_3. Similar to YSZ, many polyhedral ZrO_2 phases also present at the surface of the corroded 4.5Sc1.5YSZ sample, but the sizes become a bit larger. Moreover, a close look at the granular grains indicates some corrosion pits can be observed on the grain surfaces. The corrosion pits may be attributed to the corrosion of ZrO_2 during the formation of YVO_4 grains. In all, the addition of Sc_2O_3 can greatly change the corrosive sample morphologies.

The surface morphologies of 5.5Sc1.5YSZ ceramics after hot corrosion in Na_2SO_4 + V_2O_5 salts for 100h at 1000 °C , as shown in Figs. 6e and f, are very close to that of 4.5Sc1.5YSZ. However, the granular corrosion product of YVO_4 becomes much less and smaller compared to that on the corroded surface of 4.5Sc1.5YSZ ceramics. Small corrosion pits can also be seen on the grain surface (Fig. 6e). Besides, the size of the polyhedron ZrO_2 phase is slightly larger than that formed in the 4.5Sc1.5YSZ ceramics.

The amount of granular YVO_4 phase on the surface of 6.5Sc1.5YSZ ceramics after 100h hot corrosion is much less than that on all the other specimens, as shown in Figs. 6g and h. The size is only about 3 μm in diameter. In general, no polyhedral ZrO_2 phases but the equiaxed ones can be seen at the surface of 6.5Sc1.5YSZ ceramics. Corrosion pits can be observed on the ZrO_2 phases, indicating that the ceramic surface was slightly corroded by the molten salts. And some undamaged gain boundaries of the ZrO_2 phase after 100h corrosion as shown in Fig. 6h further proves the excellent corrosion resistance of 6.5Sc1.5YSZ.

Figs. 7a and b show the cross-sectional morphologies of YSZ ceramics after hot corrosion in the Na_2SO_4 + V_2O_5 molten salts for 100 h at 1000 °C. An about 60 μm-

thick corrosion zone in the surface layer can be clearly observed. The holes in the corrosion region are filled with vanadates, where is defined as the vanadate-rich zone due to the abundance of V_2O_5 and $NaVO_3$. About 14.0 at.% V, 0.6at.% Na and 13.6 at.% Y are detected in region J marked in Fig. 7b. Since both V_2O_5 and $NaVO_3$ have low melting points of 690 °C and 610 °C, respectively, the vanadate salts have excellent mobility and permeability at 1000 °C. This allows the molten vanadates to penetrate into the inner YSZ ceramics through micro-cracks and open pores, and then to react with Y_2O_3 to form YVO_4. The resulted Y depletion in the YSZ substrate results in the t-ZrO_2 to m-ZrO_2 phase transformation.

The corresponding corrosion zones of the corroded 4.5Sc1.5YSZ and the 5.5Sc1.5YSZ ceramics are about 8 and 6 μm, respectively, in depth (Figs. 7c-f) which are much less than that of the 4.5YSZ ceramics. It clearly indicates that the addition of Sc_2O_3 to zirconia seems to have the capability to effectively prohibit the penetration of vanadates into the inner ScYSZ ceramics, and greatly improve the corrosion resistance in the molten vanadate salts at elevated temperatures. As for 6.5Sc1.5YSZ, no such surface corrosion zone exists, as shown in Figs. 7g and h. This further proves little attack to 6.5Sc1.5YSZ by the molten salts at high temperature. The material exhibits excellent performance in hot corrosion resistance to the Na_2SO_4 + V_2O_5 molten salts at elevated temperature.

The elemental distributions across the cross-sections of the samples under current investigation are shown in Fig. 8. The corroded YSZ ceramics clearly show a roughly 60 μm-thick corrosion zone of which the top ~12 μm layer is barely Y and V detectable and the lower 50 μm is rich in V resulted from vanadate penetration (Fig.

8a). Actually the penetration depth of V can be more than 100 μm. The penetration of vanadates (especially the $NaVO_3$) improves the Y^{3+} diffusion mobility [9], and therefore promotes the leaching of Y from the zirconia substrate and the growth of the corrosion product as YVO_4 on the surface of the ceramics. As a consequence, tetragonal-to-monoclinic phase transformation occurs, which results in the degradation of anti-corrosion performance for the ceramics. For ScYSZ ceramics with low Sc content less than 5.5mol.% (Figs.8 b and c), the depths of V element penetration are much less than that in 4.5YSZ, which indicates that the addition of Sc_2O_3 to ZrO_2 can greatly prohibit the vanadate penetration and its further damages to the substrate. Further increase of Sc_2O_3 can make such effect more apparent. Only little V can be detected within the top layer of 6.5Sc1.5YSZ ceramics, whereas a lot of V present on the sample surface (Fig.8 d). All these findings show that the hot corrosion resistance to the Na_2SO_4 + V_2O_5 molten salts increases with the Sc_2O_3 addition to zirconia, and the obtained ScYSZ ceramic becomes almost immune to the attack of the molten salts when the doped Sc_2O_3 amount is more than 6.5 mol.%.

A schematic of the corrosion behavior of ScYSZ ceramics in the Na_2SO_4 + V_2O_5 molten salts at 1000 °C can be illustrated as Fig. 9, based on the analysis presented above. The depth of vanadate penetration and the resulted grain shapes and amounts of the corrosion products vary with the doping levels of Sc_2O_3 in ScYSZ. For example, vanadates penetrate into the substrate much deeper with no Sc_2O_3 doping in the ceramics. The corrosion products of YVO_4 appear bar-shapes in YSZ and turn into granular shapes along with the amount reduction when more Sc_2O_3 is doped in YSZ. Significant amount of YVO_4 formation usually causes the obvious Y-depletion and results in the phase transformation of t-ZrO_2 to m-ZrO_2 in the top surface layers, and

therefore a severe corrosion behavior.

3.3. Mechanism analysis

Numerous studies have been conducted on the corrosion behavior of the YSZ ceramic coatings with different dopants in molten salts containing vanadium and sulfur [6-9, 13, 28, 43]. It is reported that the ScYSZ ceramics can be corroded by the molten salts of V_2O_5 + $NaVO_3$ due to the mineralization effect [44]. When the sample surfaces are exposed to the Na_2SO_4 + V_2O_5 molten salts at 1000 °C, many chemical reactions will occur. Firstly, Na_2SO_4 can promote the formation of an intermediate product, $NaVO_3$, which has a low melting point of ~ 610 °C through the reaction between Na_2SO_4 and V_2O_5 at 1000 °C, as described in Eq. 6. The existence of $NaVO_3$ enhances the activity and migration of V^{5+} ion and rare earth cations (RE^{3+}), which promotes the severe reactions between the rare earth oxides (RE_2O_3) and the corrosive salts. More clearly, $NaVO_3$ reacts with RE_2O_3 in ZrO_2 to form the corrosion products such as $REVO_4$ crystal and the monoclinic ZrO_2 (m- ZrO_2) (Eq. 7), and V_2O_5 reacts with RE_2O_3 to form $REVO_4$ (Eq. 8). The resultant SO_3 in Eq. 6 and Na_2O in Eq. 7 can produce Na_2SO_4 back. In other words, Na_2SO_4 in the molten salts acts as a catalyst during the hot corrosion test in this work [45].

$$V_2O_5(l) + Na_2SO_4(l) \rightarrow 2NaVO_3(l) + SO_3(g) \quad (6)$$

$$ZrO_2(RE_2O_3)(s) + 2NaVO_3(l) \rightarrow m\text{ - }ZrO_2(s) + 2REVO_4(s) + Na_2O(l) \quad (7)$$

$$V_2O_5(l) + RE_2O_3(s) \rightarrow 2REVO_4(s) \quad (8)$$

$$SO_3(g) + Na_2O(l) \rightarrow Na_2SO_4(l) \quad (9)$$

By combining the above reactions, the overall corrosion reaction in this study can be described by Eq. 10 and Eq. 11 as follows. It should be noted that the reaction involves the dissolution of the rare earth elements (RE) from the tetragonal ZrO_2. The

possible reaction between ZrO_2 and V_2O_5 is also listed as Eq. 12.

$$V_2O_5(l) + Y_2O_3(s) \rightarrow 2YVO_4(s) \quad (10)$$

$$V_2O_5(l) + Sc_2O_3(s) \rightarrow 2ScVO_4(s) \quad (11)$$

$$V_2O_5(l) + ZrO_2(s) \rightarrow ZrV_2O_7(s) \quad (12)$$

It is well known that the reaction between V_2O_5 and the ceramic oxides follows the Lewis acid-base rule. Among Y_2O_3, Sc_2O_3 and ZrO_2, Y_2O_3 has the strongest basicity and therefore the acidic V_2O_5 will preferentially react with it to form YVO_4. Relatively, Sc_2O_3 is an oxide with weak basicity, which implies its inertness to be corroded by V_2O_5 and keeps the zirconia substrate maintain the phase stability.

To better illustrate the corrosion behavior in a system of ScYSZ and Na_2SO_4 + V_2O_5 molten salts, the Gibbs free energies (ΔG) of the above reactions at 1000 °C are calculated with $\Delta_r G_m = \Delta_r H_m - T\Delta_r S_m$, $\Delta_r H_m = \sum \Delta_f H_m^{products} - \sum \Delta_f H_m^{reactants}$, and $\Delta_r S_m = \sum \Delta_f S_m^{products} - \sum \Delta_f S_m^{reactants}$. The relevant enthalpies and entropies of formation of the chemicals used for ΔG calculations are obtained from the literatures [46-48]. The Gibbs free energy of $NaVO_3$ formation is about -12.45 KJ /mol at 1000 °C, and those values for the formation of YVO_4, $ScVO_4$, and ZrV_2O_7 are -238.05 KJ /mol, 47.86 KJ/mol and -60.71 KJ /mol, respectively. From the calculated ΔG values, one can determine Y_2O_3 is preferential to react with V_2O_5 to form YVO_4 and Sc_2O_3 is hard to react with V_2O_5, which is consistent with the results according to the Lewis acid-base rule. Rather, ZrO_2 could react with V_2O_5 to form ZrV_2O_7 at 1000 °C due to its negative ΔG value, ZrV_2O_7 tends to decompose into a mixture of ZrO_2 and liquid V_2O_5 when the temperature is above 747 °C [49]. In other words, $ScVO_4$ and ZrV_2O_7 are unlikely to present physically at the temperature of 1000 °C. As a result,

no evidence of such chemicals can be observed in the samples in current study.

4. Conclusion

Doping with Sc_2O_3 in the YSZ ceramics can increase its hot corrosion resistance to the Na_2SO_4 + V_2O_5 molten salts at 1000 °C. The morphologies and amounts of the corrosion products vary with the Sc_2O_3 content. Significant amount of the main the corrosion product, YVO_4, appears in bar-shaped configurations at the surface of the corroded YSZ ceramics, while it turns into granular shapes with reduced amounts when more Sc_2O_3 doped in YSZ. The formation of YVO_4 is mainly due to the relatively easy reaction of the vanadates which penetrate into the substrate with Y leached from the substrate lattice. Leaching of Y will further result in the tetragonal-to-monoclinic transformation. Introduction of Sc_2O_3 into YSZ can enhance the M-O bond strength and the substrate's ability to prohibit the vanadate penetration due to its relatively shorter ionic radius of Sc^{3+} than that of Y^{3+} and Zr^{4+}. Furthermore, the least possibility to react Sc_2O_3 with V_2O_5, according to the Gibbs free energy calculation and the Lewis acid-base rule, promotes the phase stability of the ScYSZ ceramics. The excellent hot corrosion resistance can be achieved for those ScYSZ ceramics with higher Sc_2O_3 content, such as 6.5Sc1.5YSZ.

Acknowledgments

This work is supported by Guangxi Natural Science Foundation (Grant No. 2018GXNSFAA281176, 2016GXNSFAA380214), National Natural Science Foundation of China (Grant No. 51361003), the Youth Foundation of Guangxi Key Laboratory of Processing for Non-Ferrous Metallic and Featured Materials (Grant No. GXYSYF1801), and the Incubation Programme for thousands of Youth backbone

teachers for Guangxi institution of higher educations (The first batch).

Data Availability

References

[1] J.Y. Yuan, H. Zhang, X. Zhou, J.B. Sun, J.S. Wang, S.J. Dong, J.N. Jiang, L.H. Deng, X.Q. Cao, Phase and microstructure evolution of $SrCeO_3$ ceramic when exposed to molten V_2O_5 at 700-1250 ℃, Corros. Sci. 145 (2018) 295-306. https://doi.org/10.1016/j.corsci.2018.10.013.

[2] B.P. Zhang, W.J. Song, L.L. Wei, Y.X. Xiu, H.B. Xu, D.B. Dingwell, H.B. Guo, Novel thermal barrier coatings repel and resist molten silicate deposits, Scripta Mater. 163 (2019) 71-76. https://doi.org/10.1016/j.scriptamat.2018.12.028.

[3] N.P. Padture, Advanced structural ceramics in aerospace propulsion, Nat. Mater. 15 (2016) 804-809. https://doi.org/10.1038/nmat4687.

[4] J. Zhang, X.Y. Guo, Y.G. Jung, L. Li, J. Knapp, Lanthanum zirconate based thermal barrier coatings: A review, Surf. Coat. Technol. 323 (2017) 18-29. https://doi.org/10.1016/j.surfcoat.2016.10.019.

[5] C.A. Macauley, A.N. Fernandez, C.G. Levi, Phase equilibria in the ZrO_2-$YO_{1.5}$-$TaO_{2.5}$ system at 1500 ˚C, J. Eur. Ceram. Soc. 37 (2017) 4888-4901. https://doi.org/10.1016/j.jeurceramsoc.2017.06.031.

[6] J. Wang, Y.Z. Zhou, X.Y. Chong, R. Zhou, J. Feng, Microstructure and thermal properties of a promising thermal barrier coating: $YTaO_4$, Ceram. Int. 42 (2016) 13876-13881. https://doi.org/10.1016/j.ceramint.2016.05.194.

[7] X.R. Ren, W. Pan, Mechanical properties of high-temperature-degraded yttria-stabilized zirconia, Acta Materialia, 69 (2014) 397-406.

https://doi.org/10.1016/j.actamat.2014.01.017.

[8] R. Ahmadi-Pidani, R. Shoja-Razavi, R. Mozafarinia, H. Jamali, Evaluation of hot corrosion behavior of plasma sprayed ceria and yttria stabilized zirconia thermal barrier coatings in the presence of Na_2SO_4 + V_2O_5 molten salt, Ceram. Int. 38 (2012) 6613-6620. https://doi.org/10.1016/j.ceramint.2012.05.047.

[9] M.H. Habibi, L. Wang, J.D. Liang, S.M. Guo, An investigation on hot corrosion behavior of YSZ-Ta_2O_5 in Na_2SO_4+V_2O_5 salt at 1100 °C, Corros. Sci. 75 (2013) 409-414. https://doi.org/10.1016/j.corsci.2013.06.025.

[10] L. Wang, D.C. Li, J.S. Yang, F. Shao, X.H. Zhong, H.Y. Zhao, K. Yang, S.Y. Tao, Y. Wang, Modeling of thermal properties and failure of thermal barrier coatings with the use of finite element methods: a review, J. Eur. Ceram. Soc. 36 (2016) 1313-1331. https://doi.org/10.1016/j.jeurceramsoc.2015.12.038.

[11] H. Jamali, R. Mozafarinia, R. Shoja-Razavi, R. Ahmadi-Pidani, Comparison of hot corrosion behaviors of plasma-sprayed nanostructured and conventional YSZ thermal barrier coatings exposure to molten vanadium pentoxide and sodium sulfate, J. Eur. Ceram. Soc. 34 (2014) 485-492. https://doi.org/10.1016/j.jeurceramsoc.2013.08.006.

[12] M. Nejati, M.R. Rahimipour, I. Mobasherpour, Evaluation of hot corrosion behavior of CSZ, CSZ/micro Al_2O_3, and CSZ/nano Al_2O_3, plasma sprayed thermal barrier coatings, Ceram. Int. 40 (2014) 4579-4590. https://doi.org/10.1016/j.ceramint.2013.08.135.

[13] L. Guo, C.L. Zhang, Q. He, Z.H. Li, J.X. Yu, X.C. Liu, F.X. Ye, Corrosion products evolution and hot corrosion mechanisms of $REPO_4$ (RE=Gd, Nd, La) in the presence of V_2O_5 + Na_2SO_4 molten salt, J. Eur. Ceram. Soc. 39 (2019) 1496-1506. https://doi.org/10.1016/j.jeurceramsoc.2018.10.031.

[14] R. Ahmadi-Pidani, R. Shoja-Razavi, R. Mozafarinia, H. Jamali, Comparison of Hot Corrosion Resistance of YSZ and CYSZ Thermal Barrier Coatings in Presence of Sulfate-Vanadate Molten Salts, Advan. Mater. Research. 472-475 (2012) 141-144. https://doi.org/10.4028/www.scientific.net/AMR.472-475.141.

[15] M.R. Loghman-Estarki, M. Nejati, H. Edris R.S. Razavi, H. Jamali, A. H. Pakseresht, Evaluation of hot corrosion behavior of plasma sprayed scandia and yttria co-stabilized nanostructured thermal barrier coatings in the presence of molten sulfate and vanadate salt, J. Eur. Ceram. Soc. 35 (2015) 693-702. https://doi.org/10.1016/j.jeurceramsoc.2014.08.029.

[16] M.H. Habibi, S.M. Guo, The hot corrosion behavior of plasma sprayed zirconia coatings stabilized with yttria, ceria, and titania in sodium sulfate and vanadium oxide, Mater. Corros. 66 (2015) 270-277. https://doi.org/10.1002/maco.201307331.

[17] L. Guo, C. Zhang, M. Li, W. Sun, Z.Y Zhang, F.X. Ye, Hot corrosion evaluation of Gd_2O_3-Yb_2O_3, co-doped Y_2O_3, stabilized ZrO_2, thermal barrier oxides exposed to Na_2SO_4 + V_2O_5, molten salt, Ceram. Int. 43 (2017) 2780-2785. https://doi.org/10.1016/j.ceramint.2016.11.109.

[18] Y.X. Wang, C.G. Zhou, Hot corrosion behavior of nanostructured Gd_2O_3 doped YSZ thermal barrier coating in presence of Na_2SO_4 + V_2O_5 molten salts, Prog. Nat. Sci. Mater. 27 (2017) 507-513. https://doi.org/10.1016/j.pnsc.2017.06.010.

[19] H.F. Liu, S.L. Li, Q.L. Li, Y.M. Li, Investigation on the phase stability, sintering and thermal conductivity of Sc_2O_3-Y_2O_3-ZrO_2 for thermal barrier coating application, Mater. Des. 31 (2010) 2972-2977. https://doi.org/10.1016/j.matdes.2009.12.019.

[20] M.R. Loghman-Estarki, R.S. Razavi, , R. Ashiri, Effect of scandia content on the thermal shock behavior of SYSZ thermal sprayed barrier coatings, Ceram. Int. 42, (2016)11118-11125. https://doi.org/10.1016/j.ceramint.2016.04.018.

[21] R. L. Jones, D. Mess, Improved tetragonal phase stability at 1400°C with scandia, yttria-stabilized zirconia, Surf. Coat. Technol. 86-87 (1996) 94-101. https://doi.org/10.1016/S0257-8972(96)03006-X.

[22] W. Fan, Y. Bai, Z.Z. Wang, J.W. Che, Y. Wang, W.Z. Tao, R.J. Wang, G.Y. Liang, Effect of point defects on the thermal conductivity of Sc_2O_3-Y_2O_3 co-stabilized tetragonal ZrO_2 ceramic maerials, J. Eur. Ceram. Soci. 39 (2019) 2389-2396. https://doi.org/10.1016/j.jeurceramsoc.2019.02.034.

[23] M. Leoni, R.L. Jones, P. Scardi, Phase stability of Scandia-yttria-stabilized zirconia TBCs, Surf. Coat. Technol. 108-109 (1998) 107-113. https://doi.org/10.1016/S0257-8972(98)00617-3.

[24] R.L. Jones, R.F. Reidy, D. Mess, Scandia, Yttria-stabilized zirconia for thermal barrier coatings, Surf. Coat. Technol. 82 (1996) 70-76. https://doi.org/10.1016/0257-8972(95)02646-0.

[25] R.L. Jones, Scandia-stabilized zirconia for resistance to molten vanadate-sulfate corrosion, Surf. Coat. Technol. 39-40 (1989) 89-96. https://doi.org/10.1016/0257-8972(89)90044-3.

[26] M.R. Loghman-Estarki, R.S. Razavi, H. Edris, S.R. Bakhshi, M. Nejati, H. Jamali, Comparison of hot corrosion behavior of nanostructured ScYSZ and YSZ thermal barrier coatings, Ceram. Int. 42 (2016) 7432-7439. https://doi.org/10.1016/j.ceramint.2016.01.147.

[27] H.F. Liu, X. Xiong, X.B. Li, Y.L. Wang, Hot corrosion behavior of Sc_2O_3-Y_2O_3-ZrO_2 thermal barrier coatings in presence of $Na_2SO_4 + V_2O_5$ molten salt, Corros. Sci. 85 (2014) 87-93. https://doi.org/10.1016/j.corsci.2014.04.001.

[28] X.L. Chen, Y. Zhao, L.J. Gu, B.L. Zou, Y. Wang, X.Q. Cao, Hot corrosion behaviour of plasma sprayed YSZ/$LaMgAl_{11}O_{19}$ composite coatings in molten sulfate-

vanadate salt, Corros. Sci. 53 (2011) 2335-2343. https://doi.org/10.1016/j.corsci.2011.03.019.

[29] L. Guo, C.L. Zhang, L.M. Xu, M.Z. Li, Q. Wang, F.X. Ye, C.Y. Dan, V. Ji, Effects of TiO_2 doping on the defect chemistry and thermo-physical properties of Yb_2O_3 stabilized ZrO_2, J. Eur. Ceram. Soc. 37 (2017) 4163-4169. https://doi.org/10.1016/j.jeurceramsoc.2017.04.065.

[30] J.M. Cairney, N.R. Rebollo, M. Rühle, C. G. Levi, Phase stability of thermal barrier oxides: A comparative study of Y and Yb additions, Int. J. Mater. Res. 98 (2007) 1177-1187. https://doi.org/10.3139/146.101595.

[31] V. Babić, M. Ivanda, G. Štefanić, Phase development in the metastable solid solutions of ZrO_2-$YO_{1.5}$ system, J. Molec. Struct. 1185 (2019) 310-322. https://doi.org/10.1016/j.molstruc.2019.02.100.

[32] M.D. Chambers, D.R. Clarke, Effect of long term, high temperature aging on luminescence from Eu-doped YSZ thermal barrier coatings, Surf. Coat. Technol. 201 (2006) 3942-3946. https://doi.org/10.1016/j.surfcoat.2006.08.011.

[33] N.I. Baklanova, B.A. Kolesov, T.M. Zima, Raman study of yttria-stabilized zirconia interfacial coatings on Nicalon^{TM} fiber, J. Eur. Ceram. Soc. 27 (2007) 165-171. https://doi.org/10.1016/j.jeurceramsoc.2006.04.151.

[34] Y. Hemberger, C. Berthold, K.G. Nickel, Simultaneous phase and chemistry analysis in YSZ by Raman Spectroscopy, USB. Stick Unitecr. 468 (2015) 1-4.

[35] B.M. Jin, S. Erdei, A.S. Bhalla, F.W.Ainger, Raman study of oxygen deficient YVO_4, single crystals, Mater. Resear. Bullet. 30 (1995) 1293-1300. https://doi.org/10.1016/0025-5408(95)00126-3.

[36] L.L. Sun, H.B. Guo, H.Peng, S.K. Gong, H.B. Xu, Influence of partial substitution of Sc_2O_3 with Gd_2O_3 on the phase stability and thermal conductivity of

Sc_2O_3-doped ZrO_2, Ceram. Int. 39 (2013) 3447-3451. https://doi.org/10.1016/j.ceramint.2012.09.100.

[37] M.R. Loghman-Estarki, R.S. Razavi, H. Edris, M. Pourbafrany, H. Jamali,R. Ghasemi, Life time of new SYSZ thermal barrier coatings produced by plasma spraying method under thermal shock test and high temperature treatment, Ceram. Int. 40 (2014) 1405-1414. https://doi.org/10.1016/j.ceramint.2013.07.023.

[38] W. Fan, Z.Z. Wang, Y. Bai, J.W. Che, R.J. Wang, F. Ma, W.Z. Tao, G.Y. Liang, Improved properties of scandia and yttria co-doped zirconia as a potential thermal barrier material for high temperature applications, J. Eur. Ceram. Soc. 38 (2018) 4502-4511. https://doi.org/10.1016/j.jeurceramsoc.2018.06.002.

[39] O. Z. Matthew, M. Licia, J.B. Daniel, W.G. Robin, E.S. Kurt, Defect cluster formation in M_2O_3-doped cubic ZrO_2, Solid State Ionics. 128 (2000) 243-254. https://doi.org/10.1016/S0167-2738(99)00348-3.

[40] L. Guo, M.Z. Li, F.X. Ye, Phase stability and thermal conductivity of RE_2O_3 (RE=La, Nd, Gd, Yb) and Yb_2O_3 co-doped Y_2O_3 stabilized ZrO_2 ceramics, Ceram. Int. 42 (2016) 7360-7365. http://dx.doi.org/10.1016/j.ceramint.2016.01.138.

[41] S.A. Tsipas, Effect of dopants on the phase stability of zirconia-based plasma sprayed thermal barrier coatings, J. Eur. Ceram. Soc. 30 (2010) 61-72. https://doi.org/10.1016/j.jeurceramsoc.2009.08.008.

[42] R.D. Shannon, Revised effective ionic radii and systematic studies of interatomic distances in halides and chalcogenides, Acta. Cryst. 32 (1976) 751-767. https://doi.org/10.1107/S0567739476001551.

[43] Z.J. Fan, K.D. Wang, X. Dong, R.J Wang, W.Q. Duan, X.S. Mei, W.J. Wang, J.L. Cui, S. Zhang, C.Y. Xu, The role of the surface morphology and segmented cracks on the damage forms of laser re-melted thermal barrier coatings in presence of a molten

salt (Na_2SO_4 + V_2O_5), Corros. Sci. 115 (2017) 56-67. https://doi.org/10.1016/j.corsci.2016.11.011.

[44] S.Y. Park, J.H. Kim, M.C. Kim, H.S. Song, C.G. Park, Microscopic observation of degradation behavior in yttria and ceria stabilized zirconia thermal barrier coatings under hot corrosion, Surf. Coat. Technol. 190 (2005) 357-365. https://doi.org/10.1016/j.surfcoat.2004.04.065.

[45] C. Batista, A. Portinha, R.M.Ribeiro, V. Teixeira, C.R.Oliveira, Evaluation of laser-glazed plasma-sprayed thermal barrier coatings under high temperature exposure to molten salts, Surf. Coat. Technol. 200 (2006) 6783-6791. https://doi.org/10.1016/j.surfcoat.2005.10.011.

[46] Y.J. Liang, Y.C. Che, Inorganic thermodynamics data book, second ed., Northeast University Press, Shenyang, 1994.

[47] H. Yokokawa, N. Sakai, T. Kawada, M. Dokiy, Chemical Potential Diagrams for Rare Earth-Transition Metal-Oxygen Systems: I, Ln-V-O and Ln-Mn-O System, J. Am. Ceram. Soc. 73 (1990) 649-58.

https://doi.org/10.1111/j.1151-2916.1990.tb06567.x

[48] K. S. Gavrichev, M. A. Ryumin, A. V. Tyurin, V. M. Gurevich, O. I. Solov'ev, L. N. Komissarova, Thermodynamic functions of $ScVO_4$ at temperatures from 0 to 350 K, Inorganic Mater. 48 (2012) 845-850. https://doi.org/10.1134/S0020168512070059.

[49] C. L. Zhang, M.Z. Li, Y.C. Zhang, L. Guo, J.X. Dong, .X.F Ye， L.W. Li, J. Vincent, Hot corrosion behavior of $(Gd_{0.9}Sc_{0.1})_2Zr_2O_7$ in V_2O_5 molten salt at 700 - 1000 °C, Ceram. Int. 43 (2017) 9041-9046. https://doi.org/10.1016/j.ceramint.2017.04.048.

Captions

Table 1 Summary of the lattice parameters of as prepared YSZ and ScYSZ ceramics through Rietveld refinement

Table 2 The calculated m-ZrO_2 content in the YSZ and ScYSZ ceramics after hot corrosion in $Na_2SO_4 + V_2O_5$ molten salts at 1000 °C (vol.%) for various exposure time

Table 3 The chemical compositions (in at.%) of the selected regions indicated in Fig. 6 using EDS analysis

Fig. 1. XRD patterns of as-prepared YSZ and ScYSZ ceramics: (a) 20-90 ° region, (b) 72-76 ° region, and the refined XRD pattern of (c) YSZ and (d) 4.5Sc1.5YSZ.

Fig. 2. XRD patterns of the YSZ and ScYSZ ceramics after hot corrosion in $Na_2SO_4 + V_2O_5$ molten salts at 1000 °C for different time: (a) 4.5YSZ, (b) 4.5Sc1.5YSZ, (c) 5.5Sc1.5YSZ and (d) 6.5Sc1.5YSZ.

Fig. 3. The calculated m-ZrO_2 contents in the YSZ and ScYSZ ceramics after hot corrosion in $Na_2SO_4 + V_2O_5$ molten salts at 1000 °C as functions of exposure time.

Fig. 4. Raman spectra of the YSZ and ScYSZ ceramics after hot corrosion in $Na_2SO_4 + V_2O_5$ molten salts for 100 h at 1000 °C.

Fig. 5. Phase diagrams for the RE_2O_3-ZrO_2 systems: (a) Y_2O_3-ZrO_2 and (b) Sc_2O_3-ZrO_2 [33]. The red and blue dashed lines in (a) represents the mole fractions of Y in the ceramics with and without Sc_2O_3 doping, respectively. The blue dashed line in (b) represents the mole fraction of Sc in 6.5Sc1.5YSZ.

Fig. 6. Surface morphologies of the YSZ and ScYSZ ceramics after 100 h hot corrosion in $Na_2SO_4 + V_2O_5$ molten salts at 1000 °C: (a, b) YSZ; (c, d) 4.5Sc1.5YSZ;

(e, f) 5.5Sc1.5YSZ; and (g, h) 6.5Sc1.5YSZ.

Fig. 7. Cross-sectional morphologies of the YSZ and ScYSZ ceramics after 100 h hot corrosion in Na_2SO_4 + V_2O_5 molten salts at 1000 °C: (a, b) YSZ, (c, d) 4.5Sc1.5YSZ, (e, f) 5.5Sc1.5YSZ and (g, h) 6.5Sc1.5YSZ.

Fig. 8. Elemental mapping of the YSZ and ScYSZ ceramics after 100h hot corrosion in Na_2SO_4 + V_2O_5 molten salts at 1000 ^oC: (a) YSZ, (b) 4.5Sc1.5YSZ, (c) 5.5Sc1.5YSZ and (d) 6.5Sc1.5YSZ.

Fig. 9. Schematic illustrations of the corrosion behavior for the Sc_2O_3 doped YSZ ceramics: (a) YSZ, (b) ScYSZ with low Sc_2O_3 content, and (c) ScYSZ with high Sc_2O_3 content.

Table 1 Lattice parameters of as-prepared YSZ and ScYSZ ceramics through Rietveld refinement (Å)

Samples	Phases	2θ/°	a	b	c	$c/\sqrt{2}a$	vol.%
YSZ	t_1	30.096	3.6294	3.6294	5.1501	1.0034	40
	t_2	30.167	3.6075	3.6075	5.1779	1.0149	60
4.5Sc1.5YSZ	t_1	30.305	3.6025	3.6025	5.1228	1.0055	65
	t_2	30.254	3.5979	3.5979	5.1617	1.0145	35
5.5Sc1.5YSZ	t_1	30.314	3.601	3.601	5.1230	1.0060	100
6.5Sc1.5YSZ	t_1	30.325	3.6009	3.6009	5.1179	1.0050	100

Table 2 The calculated m-ZrO_2 content in the YSZ and ScYSZ ceramics after hot corrosion in $Na_2SO_4 + V_2O_5$ molten salts at 1000 °C (vol.%) for various exposure time

time/h	YSZ	4.5Sc1.5YSZ	5.5Sc1.5YSZ	6.5Sc1.5YSZ
25	94	17	13	0
50	100	46	43	0
75	100	68	65	1
100	100	84	77	1

Table 3 The chemical compositions (in at.%) of the selected regions indicated in Fig. 6 using EDS analysis

	Zr	O	Y	Sc	V	Na
A	34.8	63.8	0.0	0.0	0.8	0.6
B	0.0	42.3	27.8	0.0	29.4	0.6
C	35.1	63.6	0.0	0.5	0.6	0.2
D	0.7	62.9	17.8	1.5	16.7	0.5
E	37.8	59.8	0.0	0.8	1.2	0.5
F	0.4	44.5	25.1	2.0	27.6	0.4
G	27.5	63.7	0.7	3.8	2.0	2.3
H	0.8	48.5	23.5	2.1	24.6	0.5

Note: Due to the inevitable analytical errors pertain to the EDS evaluation, the presented data are for qualitative analysis only.

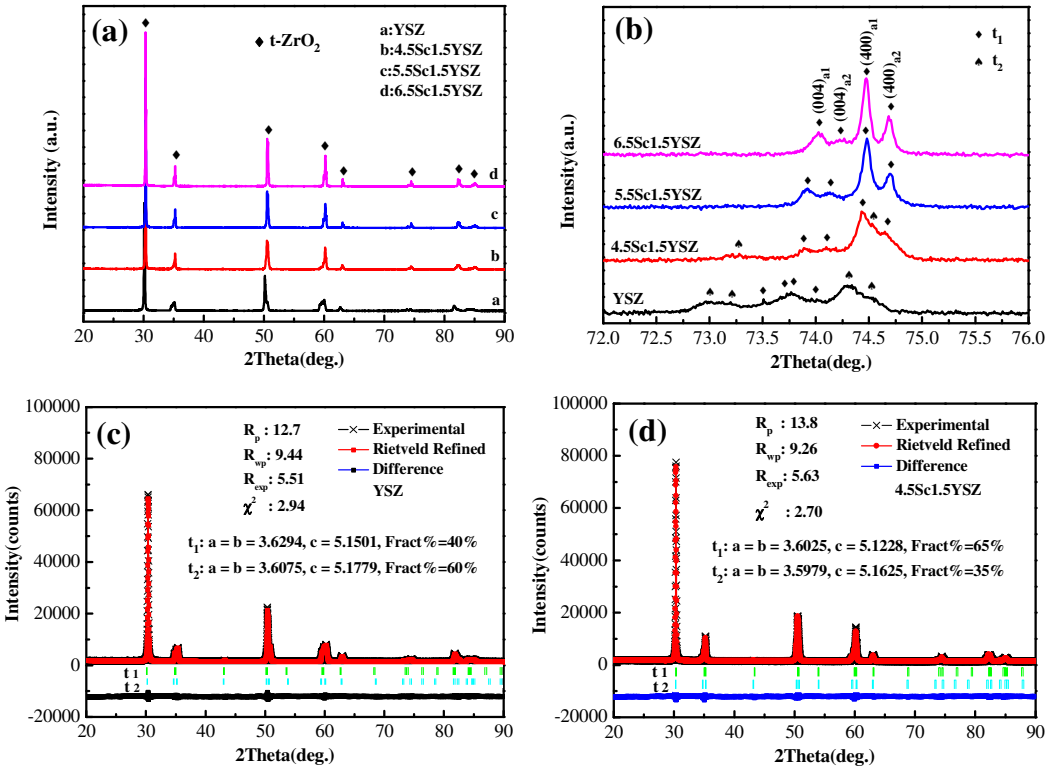

Fig. 1. XRD patterns of as-prepared YSZ and ScYSZ ceramics: (a) 20-90 ° region, (b) 72-76 ° region, and the refined XRD patterns of (c) YSZ and (d) 4.5Sc1.5YSZ.

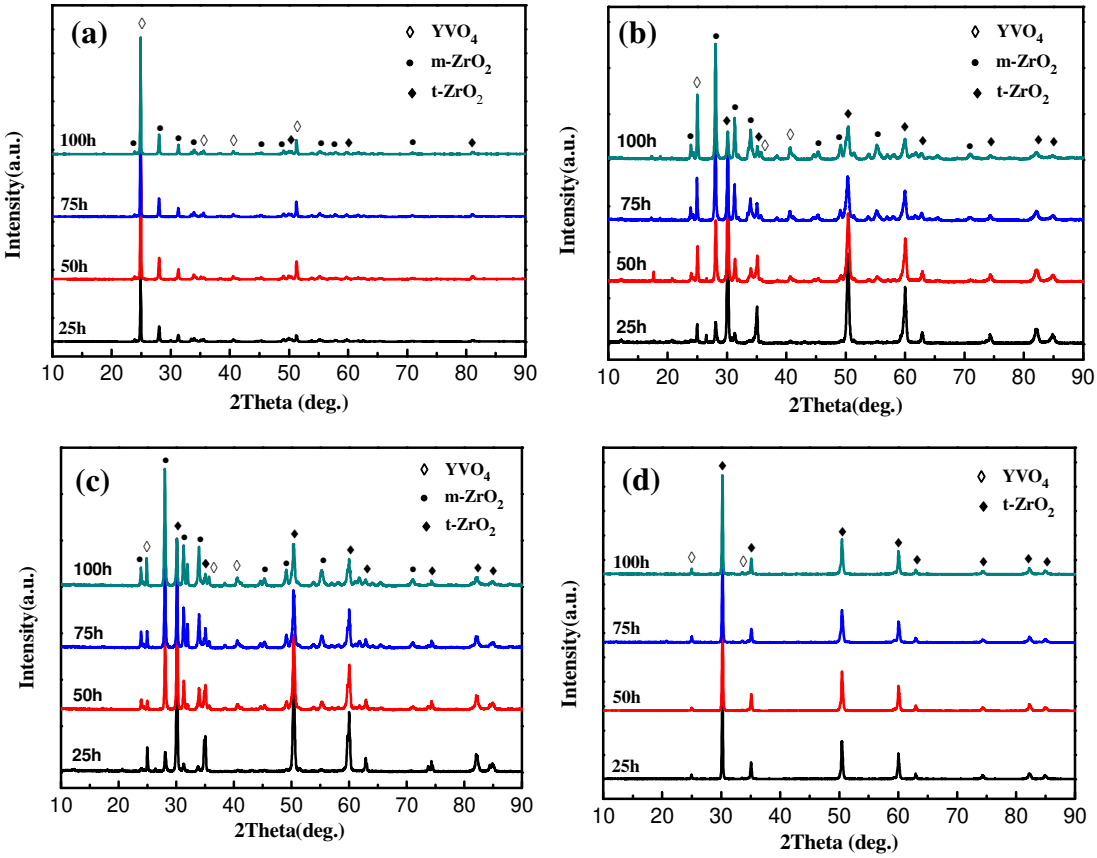

Fig. 2. XRD patterns of the YSZ and ScYSZ ceramics after hot corrosion in Na_2SO_4 + V_2O_5 molten salts at 1000 °C for different time: (a) YSZ, (b) 4.5Sc1.5YSZ, (c) 5.5Sc1.5YSZ and (d) 6.5Sc1.5YSZ.

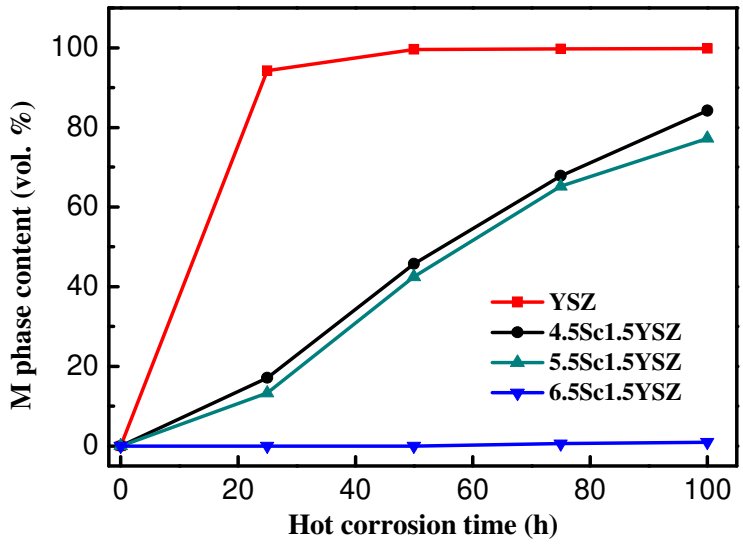

Fig. 3. The calculated m-ZrO_2 contents in the YSZ and ScYSZ ceramics after hot corrosion in $Na_2SO_4 + V_2O_5$ molten salts at 1000 °C as functions of exposure time.

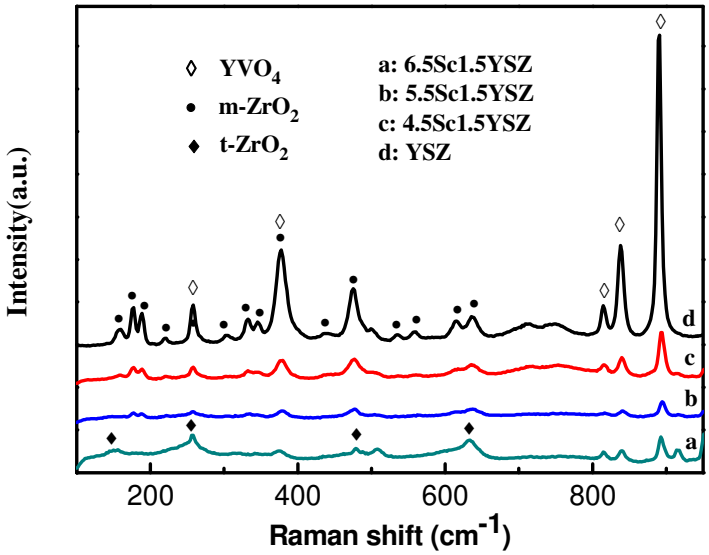

Fig. 4. Raman spectra of the YSZ and ScYSZ ceramics after hot corrosion in Na_2SO_4 + V_2O_5 molten salts for 100 h at 1000 °C.

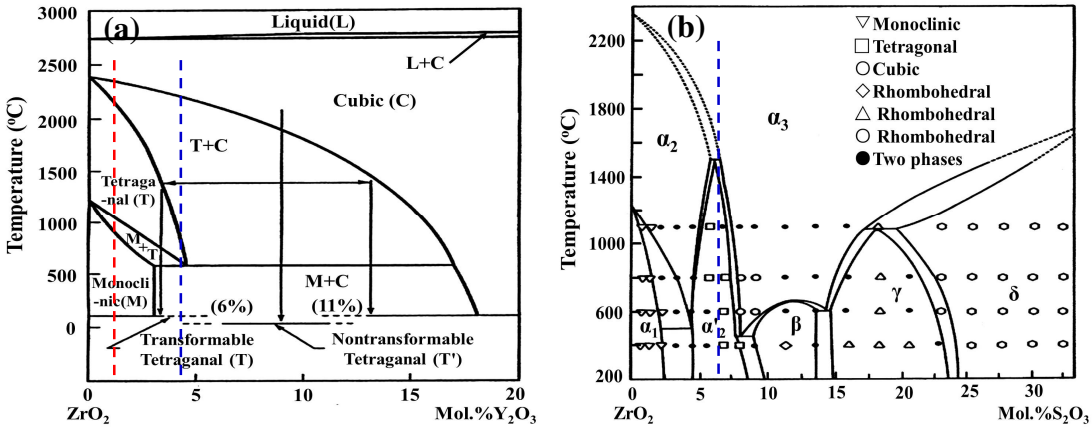

Fig. 5. Phase diagrams for the RE_2O_3-ZrO_2 systems: (a) Y_2O_3-ZrO_2 and (b) Sc_2O_3-ZrO_2 [23]. The red and blue dashed lines in (a) represents the mole fractions of Y in the ceramics with and without Sc_2O_3 doping, respectively. The blue dashed line in (b) represents the mole fraction of Sc in 6.5Sc1.5YSZ.

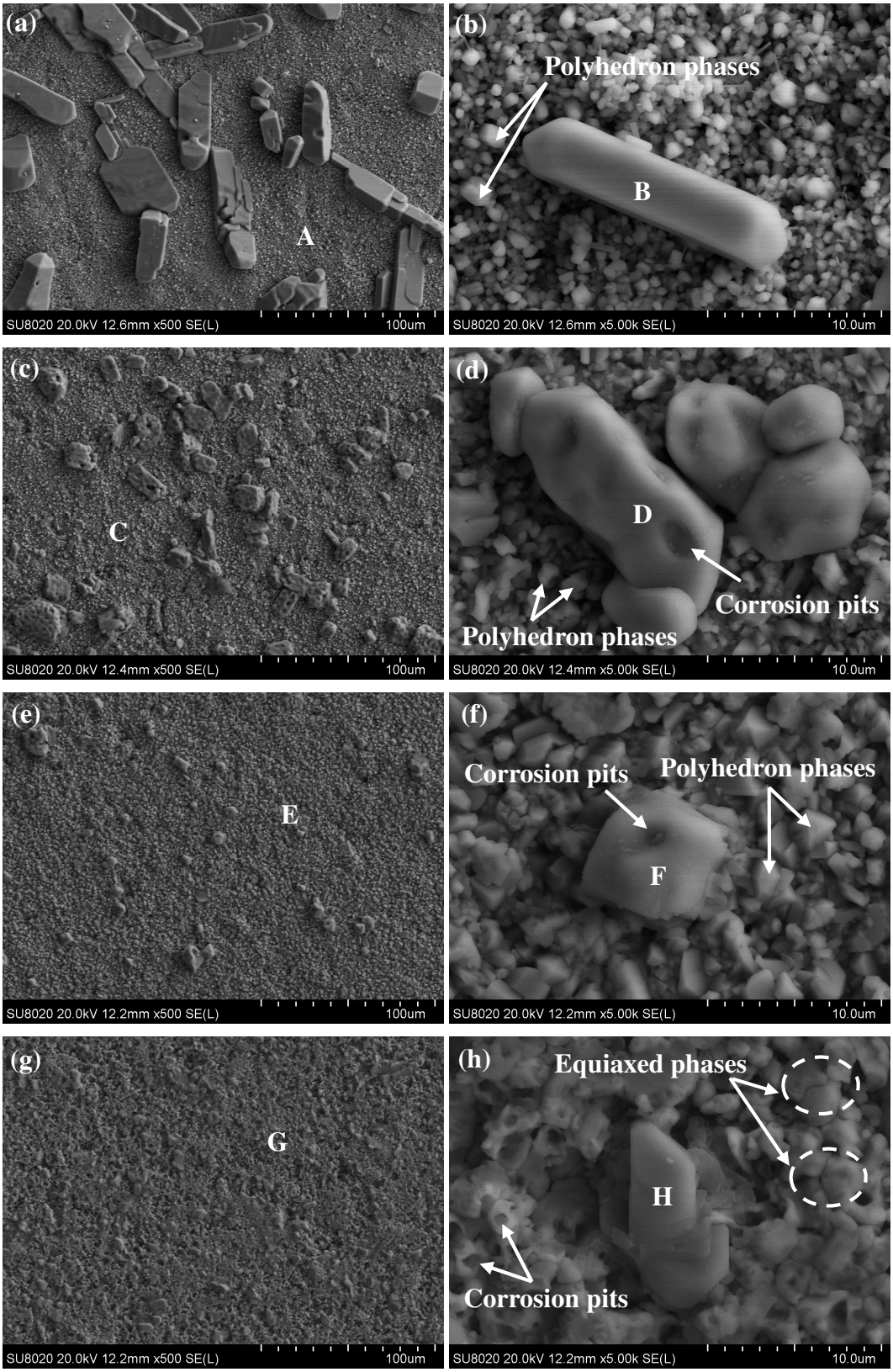

Fig. 6. Surface morphologies of the YSZ and ScYSZ ceramics after 100 h corrosion in Na_2SO_4 + V_2O_5 molten salts (a, b) YSZ, (c, d) 4.5Sc1.5YSZ, (e, f) 5.5Sc1.5YSZ and (g, h) 6.5Sc1.5YSZ.

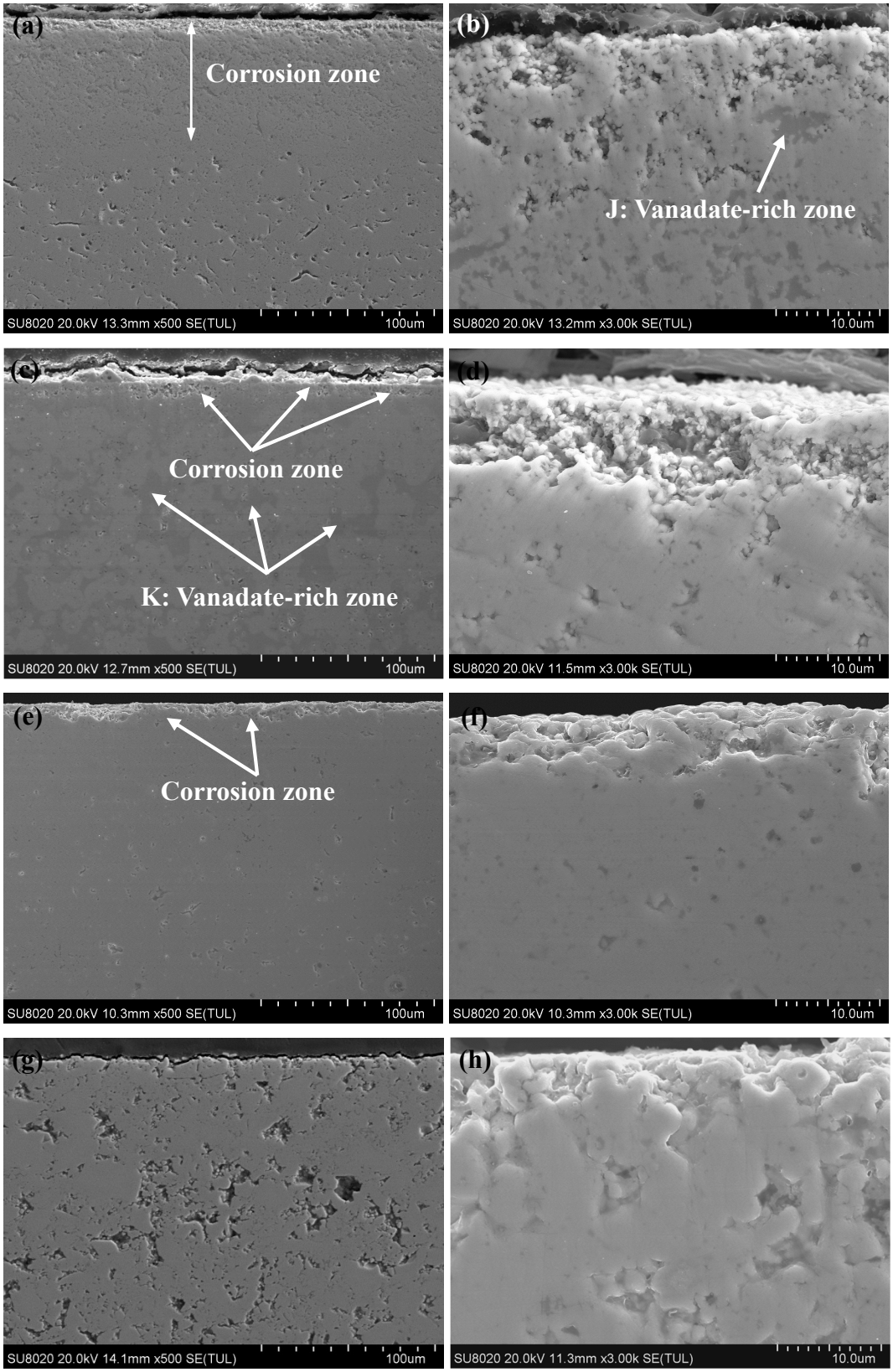

Fig. 7. Cross-sectional morphologies of the YSZ and ScYSZ ceramics after 100 h corrosion in $Na_2SO_4 + V_2O_5$ molten salts: (a, b) YSZ, (c, d) 4.5Sc1.5YSZ, (e, f) 5.5Sc1.5YSZ and (g, h) 6.5Sc1.5YSZ.

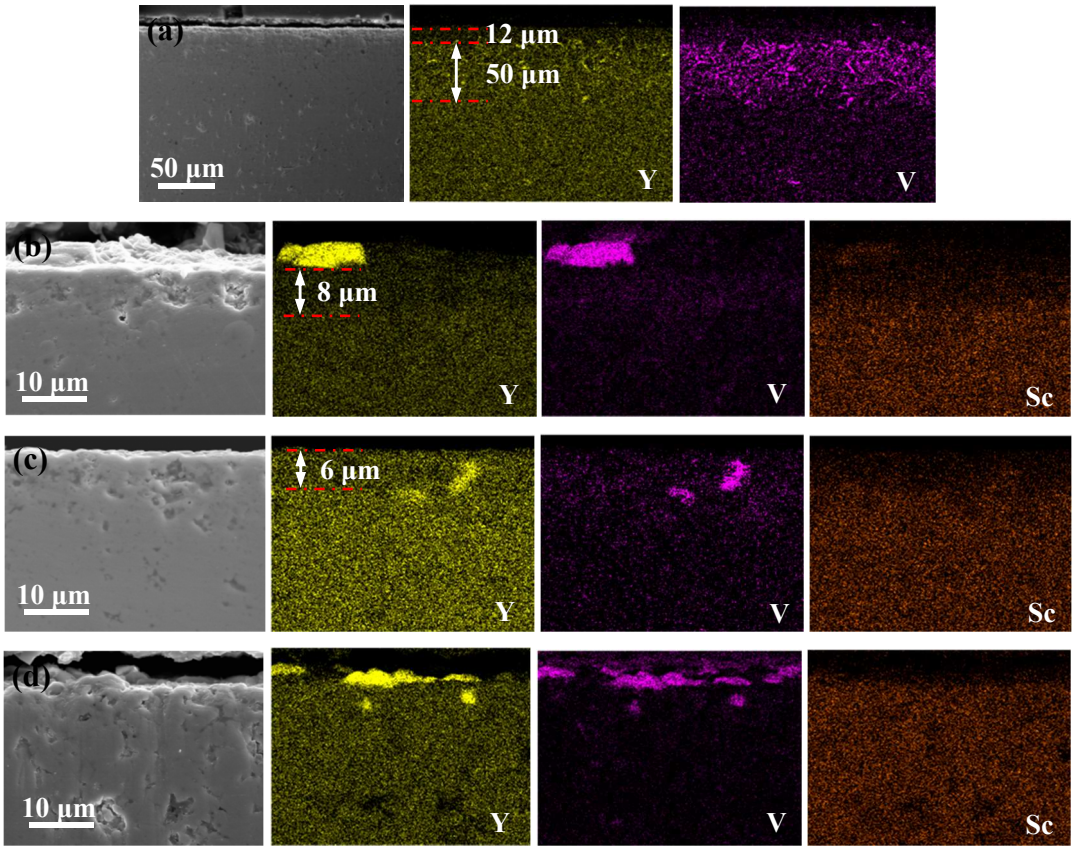

Fig. 8. Elemental mapping of the YSZ and ScYSZ ceramics after 100h hot corrosion in $Na_2SO_4 + V_2O_5$ molten salts at 1000 °C: (a) YSZ, (b) 4.5Sc1.5YSZ, (c) 5.5Sc1.5YSZ and (d) 6.5Sc1.5YSZ.

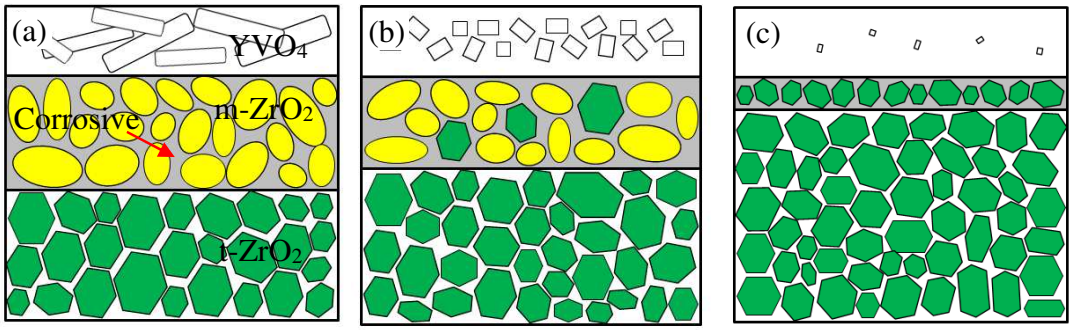

Fig. 9. Schematic illustrations of the corrosion behavior for the Sc_2O_3 doped YSZ ceramics: (a) YSZ, (b) ScYSZ with low Sc_2O_3 content, and (c) ScYSZ with high Sc_2O_3 content.